Water Research 101 (2016) 262–271

Contents lists available at ScienceDirect

Water Research

journal homepage: www.elsevier.com/locate/watres

Application of portable online LED UV fluorescence sensor to predict the degradation of dissolved organic matter and trace organic contaminants during ozonation

Wen-Tao Li [a, b], Marius Majewsky [b], Gudrun Abbt-Braun [b, *], Harald Horn [b], Jing Jin [a], Qiang Li [a], Qing Zhou [a], Ai-Min Li [a, **]

[a] State Key Laboratory of Pollution Control and Resources Reuse, School of the Environment, Nanjing University, Nanjing, 210023, China
[b] Water Chemistry and Water Technology, Karlsruhe Institute of Technology, Engler-Bunte-Ring 1, Karlsruhe 76131, Germany

ARTICLE INFO

Article history:
Received 25 March 2016
Received in revised form
27 May 2016
Accepted 28 May 2016
Available online 30 May 2016

Keywords:
Online fluorescence monitoring
Dissolved organic matter
Trace organic contaminants
Ozonation
Humic substances

ABSTRACT

This work aims to correlate signals of LED UV/fluorescence sensor with the degradation of dissolved organic matter (DOM) and trace-level organic contaminants (TOrCs) during ozonation process. Six sets of bench-scale ozonation kinetic experiments incorporated with three different water matrices and 14 TOrCs of different reactivity (group I ~ V) were conducted. Calibrated by tryptophan and humic substances standards and verified by the lab benchtop spectroscopy, the newly developed portable/online LED sensor, which measures the UV280 absorbance, protein-like and humic-like fluorescence simultaneously, was feasible to monitor chromophores and fluorophores with good sensitivity and accuracy. The liquid chromatography with organic carbon detector combined with 2D synchronous correlation analysis further demonstrated how the DOM components of large molecular weight were transformed into small moieties as a function of the decrease of humic-like fluorescence. For TOrCs, their removal rates were well correlated with the decrease of the LED UV/fluorescence signals, and their elimination patterns were mainly determined by their reactivity with O_3 and hydroxyl radicals. At approximately 50% reduction of humic-like fluorescence almost complete oxidation of TOrCs of group I and II was reached, a similar removal percentage (25–75%) of TOrCs of group III and IV, and a poor removal percentage (<25%) of group V. This study might contribute to the smart control of advanced oxidation processes for the water and wastewater treatment in the future.

1. Introduction

Diverse trace-level organic contaminants (TOrCs) including residuals of pharmaceutical and personal care products (PPCPs) and endocrine-disrupting chemicals (EDCs) have extensively been detected in wastewater effluents and drinking water sources (Behera et al., 2011; Jelic et al., 2011; Schwarzenbach et al., 2006). Prior studies have shown that such anthropogenic TOrCs can adversely affect ecological systems and are not completely eliminated by the conventional water or wastewater treatment processes (Behera et al., 2011; Jelic et al., 2011; Reungoat et al., 2010; Sui et al., 2010). With increasing public concern, the need is apparent for advanced treatment processes to improve the removal of TOrCs.

Ozonation has widely been demonstrated as an effective advanced treatment option for oxidative elimination of many TOrCs during water and wastewater treatment (Huber et al., 2003; Lee et al., 2013; Reungoat et al., 2010). Besides the direct oxidation of these pollutants by O_3, ozone decomposition also produces hydroxyl radicals (•OH) that readily react with most PPCPs and EDCs (Noethe et al., 2009; von Gunten, 2003; Wert et al., 2009). The importance of each pathway can be determined from the second order reaction rate constants between a specific contaminant and O_3 or •OH. According to their chemical reactivity, TOrCs have been operationally classified into five groups with representative compounds to assess their degradation during advanced oxidation processes (AOPs) (Gerrity et al., 2012; Lee et al., 2013).

Frequent monitoring of TOrCs is laborious, time-consuming and

* Corresponding author.
** Corresponding author.
E-mail addresses: gudrun.abbt-braun@kit.edu (G. Abbt-Braun), liaimin@nju.edu.cn, liaimingroup@nju.edu.cn (A.-M. Li).

http://dx.doi.org/10.1016/j.watres.2016.05.090
0043-1354/

expensive (Anumol et al., 2015; Chon et al., 2015; Gerrity et al., 2012). Also, given the large variety of TOrCs detected, it is impossible to monitor each one individually (Anumol et al., 2015). These difficulties can be addressed by using surrogate indicators to predict the removal efficiency of PPCP/EDC species during AOPs (Dickenson et al., 2009; Nanaboina and Korshin, 2010; Wert et al., 2009). Dissolved organic matter (DOM) plays an important role on the oxidation efficiency of TOrCs, because it is a main sink for ozone and •OH radicals (Wenk et al., 2013). The oxidation of DOM can result in the generation of low molecular weight assimilable organic carbon or biodegradable organic matter, which requires further removal by the following biological filtration (Hammes et al., 2006; Wert et al., 2008). In order to reach an appropriate oxidant dosage and to avoid under performance or high cost, simple and readily measurable parameters that provide information on the concentration and reactivity of DOM have attracted great interest in recent years. Lee et al. (2013) proposed a dissolved organic carbon (DOC)-normalized ozone dose, together with the reaction rates of selected micro-pollutants as key parameters to predict the elimination efficiency of TOrCs. Compared with DOC analysis and oxidant exposure measurements, spectral measurements are more promising for frequent online monitoring because they are relatively sensitive and easy to use. Previous bench-scale experiments have shown that the differential color, UV absorbance and fluorescence spectra are strongly correlated with the elimination of aromatic and non-aromatic TOrCs in AOPs (Chon et al., 2015; Gerrity et al., 2012; Li et al., 2013b; Nanaboina and Korshin, 2010; Wert et al., 2009). Gerrity et al. (2012) further applied an online UVA254 analyzer to illustrate how the concept can be integrated into an actual treatment train to provide real-time monitoring of process performance.

Only a few studies demonstrated the online application of fluorescence excitation emission matrix (EEM) (Carstea et al., 2010, 2016; Henderson et al., 2009), because online EEM measurement requires relatively expensive instruments and the analysis of EEM matrices also increases requirement on the data processing capacity. Generally, EEM mainly reveals two major kinds of fluorescent DOM: protein-like fluorophores and humic-like fluorophores (Li et al., 2014). The proposed total fluorescence (TF) method, which processes all the emission fluorescence peaks excited at 254 nm as a whole (Gerrity et al., 2012), might miss the different oxidation behaviors between protein-like and humic-like fluorophores. To reach a compromise between EEM and TF, monitoring protein-like and humic-like fluorescence separately is easy to operate but also informative for online application.

In addition, the commercially available online UV absorbance analyzers mainly use mercury or xenon lamps as a light source. The large size, complicated structure and expensive price are also hindering their widespread use for real-time monitoring. Hence there is strong interest to develop a cheap, small, less energy consuming but sensitive sensor, which can provide real-time feedback signals for automatic optimization of ozone dosage. Promisingly, the miniaturization of UV or fluorescence spectrometer has been advanced by the recent development of UV light-emitting diode (LED) and photodiode (PD) technology (Bridgeman et al., 2015; Dickens et al., 2011; Li et al., 2016; Tedetti et al., 2013).

The objective of this study was to apply a newly miniaturized LED UV/fluorescence sensor that we recently developed in-house to predict the degradation of DOM and the oxidation of TOrCs during ozonation. The portable online LED sensor can be used to simultaneously and continuously measure UV absorbance at 280 nm (UVA280) and protein-like and humic-like fluorescence. This study investigated 14 TOrCs of five groups of different reactivity and six sets of bench-scale ozonation kinetic experiments and three different water matrices. The degradation of TOrCs, the variation in DOM spectral characteristics, and the molecular size of DOM were analyzed. This study presents a portable/online UV/fluorescence prototype sensor for the intelligent control during advanced oxidation process.

2. Material and methods

2.1. Water matrices and TOrCs

Three water matrices and 14 TOrCs were applied, in order to provide a comprehensive and representative investigation of correlations between the spectral indices and the degradation of DOM and TOrCs. The water characteristics are shown in Table S1. The lake Hohlohsee is a brown water lake in the Black Forest, Germany, which is recharged only by precipitation and natural overflow (Frimmel et al., 2002). River sample was collected from river Rhine at Karlsruhe Maxau. And the wastewater effluent sample was taken from Karlsruhe-Neureut municipal wastewater treatment plant (WWTP). Water samples were stored at 4 °C and filtered with 0.45 μm glass fiber filters before use. The lake Hohlohsee sample was further diluted by 10 times before use.

In accordance with previous literature (Gerrity et al., 2012; Lee et al., 2013), the TOrCs were classified into five groups according to their relative reactivity with ozone and •OH radicals. As shown in Table 1, the target TOrCs in this study were: (Group I) bisphenol-A, carbamazepine, diclofenac sodium, sulfamethoxazole, triclosan and trimethoprim; (Group II) atenolol, gemfibrozil; (Group III) DEET, ibuprofen, phenytoin and primidone; (Group IV) atrazine; (Group V) TCPP.

2.2. Bench-scale ozonation experiment

Six ozonation batch experiments with three water matrices were performed in parallel tests to explore the degradation kinetics of DOM and TOrCs. For each ozonation kinetic experiment, nine or ten identical beaker flasks were filled with 500 mL of water samples and spiked with approximately 2 μg/L of each target TOrCs. Ozone was consistently generated by an oxygen-fed ozonator (Ozomat COM, Anseros, Tuebingen, Germany) and the ozone concentration was continuously monitored by an online ozone analyzer (Ozomat GM, Anseros, Tuebingen, Germany). The ~45 g/m^3 ozone gas was bubbled into the water samples with a sintered glass gas diffuser at a flow rate of 50 NL/h. In each kinetic batch, the exposure times were 0, 2, 5, 10, 20, 30, 40, 60, 100 and 300 s. For Lake Hohlohsee, it lacked the point of 40 s. Upon completion of the ozone exposure, sodium sulfite was added to quench residual ozone and the samples were then processed for analysis of DOM characteristics and TOrCs concentrations. Therefore, the ozone dosage was determined by the exposure time.

An additional experiment was performed in an ozonation reactor filled with 4 L WWTP wastewater effluent. The 45 g/m^3 O_3 gas was purged continuously at a flow rate of 50 NL/h, and the wastewater effluent was also continuously pumped in and out at a flow rate of ~100 mL/min. When the ozonized effluent was pumped out, it was led through the online UV/fluorescence sensor. The UVA280, protein-like and humic-like fluorescence were simultaneously online determined.

2.3. Analytical methods

2.3.1. Fluorescence EEM and UV absorbance

The fluorescence EEM spectra of ozonation kinetic experiments were measured with the HORIBA Aqualog spectrometer, which can simultaneously record the UV absorbance spectra. The fluorescence EEM data were processed with blank subtraction and removal of

Table 1
Information of trace organic contaminants.

Group	Contaminants [a]	CAS	$k_{[O3]}$ (M^{-1} s^{-1}), pH = 7	$k_{[^{\bullet}OH]}$ (M^{-1} s^{-1})	Functional classification
Group I – high reactivity with both ozone and ·OH					
I	Bisphenol-A	80-05-7	7×10^5	1×10^{10}	Plasticizer
I	Carbamazepine	298-46-4	3×10^5	9×10^{10}	Anticonvulsant
I	Diclofenac Sodium	15,307-86-5	1×10^6	8×10^9	nonsteroidal anti-inflammatory drugs
I	Sulfamethoxazole	723-46-6	3×10^6	6×10^9	Antibacterial/Antibiotic
I	Triclosan	3380-34-5	4×10^7	1×10^{10}	Antibacterial/Antibiotic
I	Trimethoprim	738-70-5	3×10^5	7×10^9	Antibacterial/Antibiotic
Group II – moderate reactivity with ozone and high reactivity with ·OH					
II	Atenolol	29,122-68-7	2×10^3	8×10^9	Beta-Blocker
II	Gemfibrozil	25,812-30-0	5×10^4	1×10^{10}	Lipid Regulator
Group III – low reactivity with ozone and high reactivity with ·OH					
III	DEET	134-62-3	<10	5×10^9	Herbicide/Pesticide
III	Ibuprofen	15,687-27-1	10	7×10^9	nonsteroidal anti-inflammatory drugs
III	Phenytoin	57-41-0	<10	6×10^9	Anticonvulsant
III	Primidone	125-33-7	1	7×10^9	Anticonvulsant
Group IV – low reactivity with ozone and moderate reactivity with ·OH					
IV	Atrazine	1912-24-9	6	3×10^9	Herbicide/Pesticide
Group V – low reactivity with both ozone and ·OH					
V	TCPP [b]	13,674-84-5	<1	2×10^8	Flame Retardant

[a] Compounds and rate constants refer to literature by (Gerrity et al., 2012) and (Lee et al., 2013).
[b] Flame Retardant TCEP was substituted by TCPP in this study, given that their reaction rate constants *k*-values are similar (Watts and Linden, 2009).

Raman & Rayleigh peaks. The inner filter effect (IFE) was further corrected by Aqualog software. And the EEM data in the range of Ex 220–400/Em 280–550 nm were extracted for figure drawing without further normalization.

2.3.2. LED UV fluorescence sensor

UVA280, protein-like and humic-like fluorescence signals were simultaneously measured by the portable online LED UV fluorescence sensor (Fig. S1). It uses an UV LED (280 ± 5 nm) as light source and uses UV light sensitive photodiode in line to detect the UV light that passes through the cuvette. For fluorescence detection, it uses blue light sensitive photodiodes combined with bandpass filters vertically to the UV light route to detect the fluorescence emitted from DOM. The bandpass filters were ordered with 330–355 nm for protein-like fluorescence and 415–490 nm for humic-like fluorescence. To assess its sensitivity and accuracy, calibration of the fluorescence arbitrary units was conducted with standards of L-tryptophan (≥98% purity, from Sigma-Aldrich) and humic substances (Suwannee River NOM, Catalog No. 2R101N, from International Humic Substances Society). During batch experiments, the LED sensor was operated with a quartz cuvette. And during online application, a quartz flow cell with pipe was installed. The data could be transferred onto computer via the Zigbee module and recorded by Labview software.

2.3.3. HPSEC and LC-OCD analysis

The Agilent 1200 HPSEC System equipped with Diode Array Detector (DAD) and Fluorescence Detector (FLD) was used for qualitative analysis according to our previous publications (Li et al., 2013a, 2015). The size exclusion column (SEC) PL aquagel-OH 30 (300 mm × 7.5 mm, 8 μm) was installed, and pure water was applied as the mobile phase. The DAD multi-UV absorbance scan was conducted from 200 to 300 nm with a scan step of 2 nm; while the FLD parameters for multi-emission scans were setup as Ex 280/Em 330–400 nm and Ex 280/Em 400–500 nm.

The LC-OCD analysis was performed using a TSK HW 50S (250 × 20 mm) column coupled with online UVA254 and organic carbon detectors (Huber and Frimmel, 1991). The sample injection volume was 0.5 mL, and the column was eluted with 1 mL/min phosphate buffer (1.5 g/L $Na_2HPO_4 \times 2\ H_2O$ + 2.5 g/L KH_2PO_4). The 2D correlation analysis was conducted on the LC-OCD chromatograms of ozone kinetic experiments using 2D Shige software, as described by Noda and Ozaki (2005). In addition, the chromatogram peaks were integrated and their increase or decrease along ozonation time were further calculated and correlated with the decrease of LED humic-like fluorescence.

2.3.4. LC-MS/MS analysis

Chromabond® HR-X cartridges (6 mL/200 mg) were applied for solid phase extraction (SPE). The cartridges were sequentially conditioned with acetonitrile 2 mL, methanol 4 × 2 mL and pure water 4 × 3 mL. About 400 mL of each water sample was used for SPE and the sample was weighed for concentration calculation. Before extraction, each sample was spiked with 500 μL of 1 mg/L Carbamazepine-d10 solution as internal standard to correct for losses. After extraction, the cartridges were eluted with methanol 4 × 2 mL, and the collected elutes in tubes were dried with N_2 gas. Finally, the tubes were rinsed with 1 mL acetonitrile and then the sample solution was transferred into 1.5 mL glass vials. For LC-MS/MS analysis of TOrCs, a triple-quadrupole system API3000 (Sciex) coupled to an Agilent 1100 HPLC with a Gemini C18 column from Phenomenex was applied. The MS/MS parameters are shown in Table S2. Each sample was measured with three times. Preliminary experiments showed that the extraction recoveries for all target TOrCs were of 75%–100%, and the minimal method detection limits were lower than 50 ng/L, i.e., <2.5% of the spiked concentration.

3. Results and discussion

3.1. Development of spectral surrogate parameters

3.1.1. UVA254 vs UVA280

The reduction of UV absorbance during ozone kinetic experiments is shown in Fig. 1. These results indicate that ozonation resulted in a monotonic and significant decrease in the UV absorbance spectra over 240 nm. For all water matrices, the UV differentials increased at wavelengths between 240 nm and 270 nm, and then decipherable plateaus were reached, which is consistent with previous literature data (Gerrity et al., 2012). The UVA254 has been applied to assess the degradation of PPCPs and aromatic DOM components during ozonation (Chon et al., 2015; Gerrity et al., 2012; Nanaboina and Korshin, 2010; Wert et al., 2009). However, among deep UV LEDs, the UV280 series is the most technically mature and economic, because lowering down the light

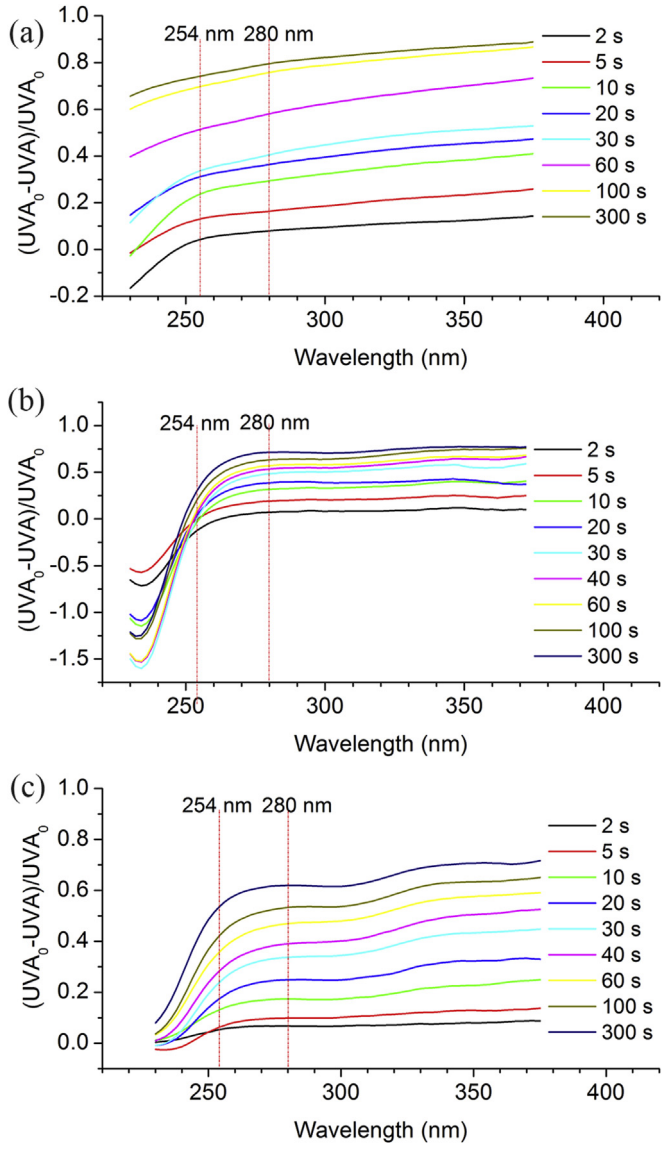

Fig. 1. The differential UV absorbance spectra of ozonation kinetic experiments: (a) Hohlohsee, (b) river Rhine and (c) WWTP effluent.

wavelength of LED is unavoidably linked to a reduction of light power and increased costs. The HPSEC multi-UV absorbance spectra (Fig. S2) indicate that both UVA254 and UVA280 reflected the same DOM species. In addition, UVA280 has been proposed over UVA254 to estimate the molecular weight and aromaticity of aquatic organic matter, which can avoid interferences with nitrate (Chin et al., 1994). These observations further confirm that UVA280 is well-suited to replace UVA254 for the evaluation of treatment efficacy.

3.1.2. LED fluorescence signals

The EEM spectra of water matrices are shown in Fig. 2. As evaluated previously, the fluorescence peaks at different excitation but similar emission wavelengths represent the same DOM fluorophores (Li et al. 2013a, 2014). Generally, the fluorescence peaks with Em > 380 nm are designated as humic-like fluorescence, associated with fluorophores that are likely to have combinations of two aromatic rings and electro-donating groups (e.g., aminonaphthol, 4-phenoxyphenol); while peaks with Em < 380 nm are attributed to protein-like fluorophores (tyrosine, tryptophan, derivatives of phenol and aniline, or the conformer of 4-phenoxyphenol) (Barsotti et al., 2016; Li et al., 2013a, 2015). The river Rhine and WWTP water matrices exhibited two protein-like peaks approximately at Ex 230, 280 nm/Em 340 nm and two humic-like peaks roughly at Ex 250, 340 nm/Em 430 nm; while lake Hohlohsee only showed humic-like fluorescence with an Em wavelength of around 450 nm. In literature, the variation of total fluorescence spectra excited at the wavelength of 254 nm was applied to reflect the behavior of DOM and TOrCs during ozonation, in which protein-like and humic-like fluorescence was calculated as a whole (Gerrity et al., 2012). However, the measurements of total fluorescence spectra increased the difficulty of online application, which requires complex light splitting system. To address this problem, the protein-like and humic-like fluorescence signals were measured independently by the combination of light filter and photodiode. Inferred from the HPSEC multi-emission fluorescence scan (Fig. S3), UV light at 280 nm can excite humic-like fluorescence as well as protein-like fluorescence. Hence the LED fluorescence sensor measures the fluorescence signals marked by the dashed circle in the EEMs (Fig. 2): the left circle (Ex 275–285 nm/Em 330–355 nm) represents the protein-like fluorescence and the right circle (Ex 275–285 nm/Em 415–490 nm) represents the humic-like fluorescence. Although the humic-like fluorescence signals were measured at their excitation slopes instead of peaks, the signals were strong enough to be proceeded by the electronic amplifying circuits.

3.1.3. Accuracy and sensitivity of LED sensor

Despite its relatively high sensitivity, the arbitrary unit of fluorescence makes it hard to compare intensity across studies. In this way, Fig. 3 shows the calibration curves of the LED UV fluorescence sensor using tryptophan and SR_NOM humic substance standards. It can be seen that all signals of the LED sensor were well linearly regressed with $R^2 > 0.99$, indicating their good accuracy. Inferred from the regression slopes, the LED protein-like fluorescence sensor was sensitive to 10 μg/L tryptophan with 7 arbitrary units, and the SR_NOM standard with a DOC concentration of 1 mg/L at

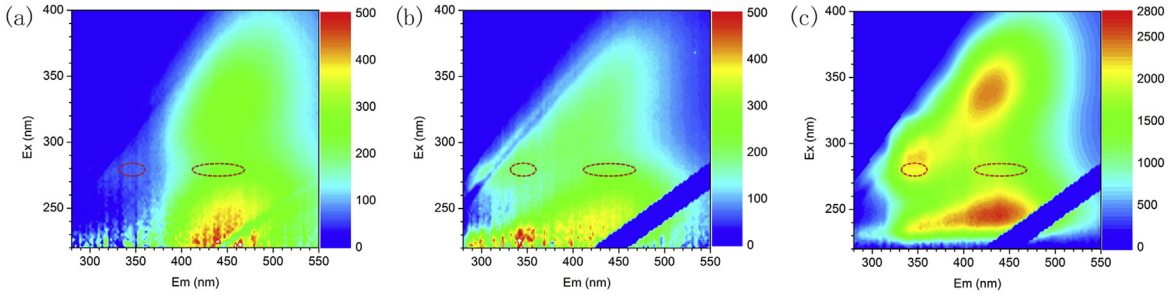

Fig. 2. The EEM spectra of (a) lake Hohlohsee, (b) river Rhine, and (c) WWTP effluent. The dashed circles represent the Ex/Em area that the LED fluorescence sensor is measuring.

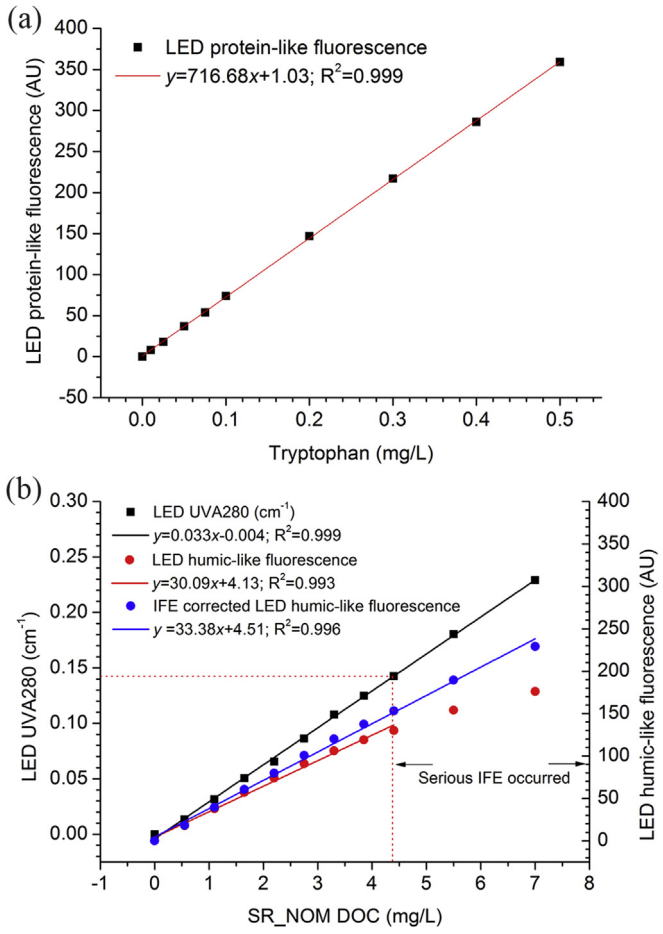

Fig. 3. Calibration of signals of LED sensor: (a) tryptophan for protein-like fluorescence and (b) SR_NOM standard for UVA280 and humic-like fluorescence.

pH = 8 resulted in ~30 LED arbitrary units of humic-like fluorescence. In addition to the accuracy and sensitivity, inner filter effect (IFE) is an important issue related to development of online fluorescence monitor. IFE consists of primary attenuation of excitation light and secondary attenuation of emitted fluorescence. The IFE affects the fluorescence intensity by the following equation:

$$F_{ideal} = F_{obs} \times 10^{\frac{Abs_{Ex}+Abs_{Em}}{2}}$$

In which, F_{obs} represents the observed fluorescence signal; Abs_{Ex} represents the absorbance value at the excitation wavelength for primary IFE correction; Abs_{Em} represents for the absorbance value at the emission wavelength for secondary IFE correction; F_{ideal} represents the IFE corrected fluorescence signal.

Inferred from Fig. 3-b, IFE occurred significantly in humic-like fluorescence when the related UVA280 was over ~0.15 cm^{-1}, and moderately when the UVA280 was in the range of 0.10–0.15 cm^{-1}. Because UVA280 values for Hohlohsee, river Rhine and WWTP water matrices were 0.082, 0.028 and 0.129 cm^{-1}, respectively, the primary IFEs in this study were not significant. Only the fluorescence signals in WWTP batch experiments were further corrected with UVA280 to abate the primary IFE. As to protein-like fluorescence, secondary IFE should be considered due to its relatively low emission wavelength. The UV absorbance values at 340 nm (representative wavelength of protein-like fluorescence) were 0.03 cm^{-1}, 0.008 cm^{-1} and 0.05 cm^{-1} for Hohlohsee, river Rhine and WWTP water matrices, respectively. Compared with the primary IFE, the secondary IFE affected protein-like fluorescence slightly across samples.

In comparison to lab benchtop spectroscopy, the correlation results in Table S3 further confirmed the good sensitivity and accuracy of LED UV fluorescence sensors for real water matrices in this study. Hereinafter, the “one LED & three signals” portable online UV/fluorescence spectrometer was applied to correlate with the degradation of DOM and TOrCs. It should be noted that the lab prototype is not mature yet. Before its industrial application, further efforts on design of structure, circuits and algorithms are needed to improve the issues related to accuracy, sensitivity, calibration and IFE.

3.2. Degradation of DOM

3.2.1. Degradation of chromophores and fluorophores

The degradation kinetics of chromophores and fluorophores were further investigated in WWTP effluent using the online LED UV/fluorescence sensor (Fig. 4), which can be described by the second order kinetic models. The curvature was likely ascribed to the dead volume in the cuvette or the diffusion effect in pipe during online measurement. It is obvious that the humic-like and protein-like fluorescence signals varied with similar kinetic equation parameters. The model slopes also suggest that fluorophores were relatively more sensitive and vulnerable than chromophores during ozonation. Since UV absorbance could be affected by residual dissolved ozone and the protein-like fluorescence is more difficult to detect than humic-like fluorescence, the humic-like fluorescence is the most promising for the future industrial application. Therefore the humic-

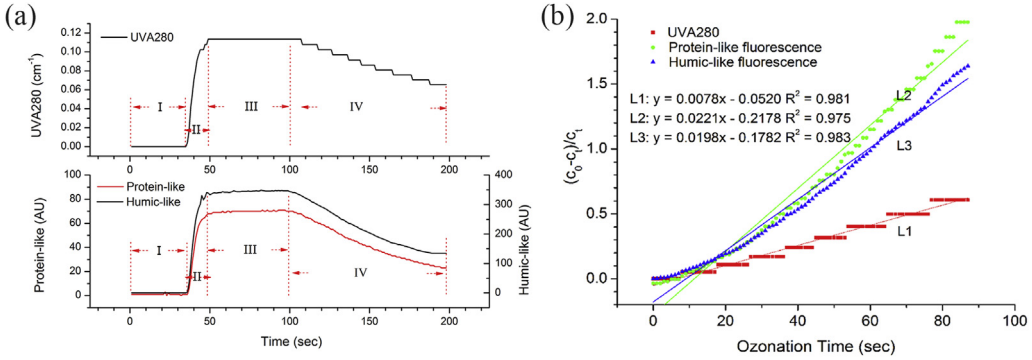

Fig. 4. The degradation kinetics of chromophores and fluorophores measured with online LED UV fluorescence monitoring. Fig. 4-(a) and (b) depict the four stages during the online UV and fluorescence monitoring: stage I, auto-zero with pure water; stage II, inflow of WWTP effluent; stage III, stable plateau; stage IV, ozonation process. The UV and fluorescence signals during stage IV was fitted to the 2nd order kinetic models in Fig. 4-(c).

like fluorescence signals were mainly discussed hereinafter.

3.2.2. Variation of DOM molecular weight

Fig. 5 shows the 2D synchronous correlation analysis of LC-OCD chromatograms of water matrices during ozonation kinetic experiments. The apparent MW references and original LC-OCD profiles are shown in Fig. S4 and Fig. S5. In the 2D synchronous correlation chromatograms, there are two types of correlation peaks, i.e., auto-peaks and cross-peaks at diagonal and off-diagonal positions, respectively. According to the Noda's rule, the auto-peaks are always positive, and their intensities represent the overall variation extent against the external perturbation variable (i.e., the ozonation time or dosage); the cross-peaks represent simultaneous or opposite changes of chromatogram peaks at two different elution times (He et al., 2014; Noda and Ozaki, 2005).

For the Hohlohsee series, there were two obvious auto-peaks centered at 39 min and 48 min on the diagonal line. The auto-peak at 48 min was selected as reference, and a horizontal auxiliary line was added to help the analysis of cross-peaks. Inferred from the contour color (blue or red), the peak a4 (52–54 min, 1–0.7 kDa) showed the simultaneous variation trend with peak a3 (45–50 min, 3–1.3 kDa); while the peaks a1 (28–30 min, >40 kDa) and a2 (34–43 min, 17–4 kDa) exhibited the opposite variation trend with peak a3. Identified by the original chromatograms (Fig. S5-a), the peaks' intensities around 48 min were significantly increasing with the increasing ozonation contact time. That means

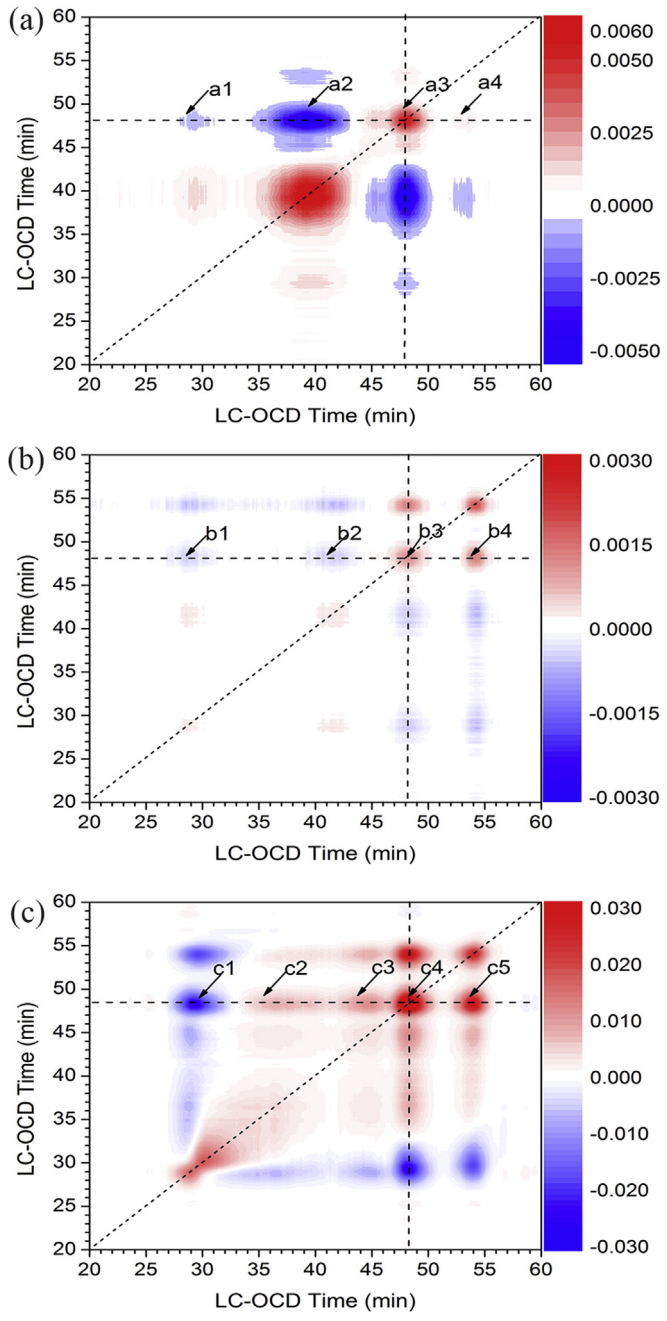

Fig. 5. The 2D synchronous correlation analysis of LC-OCD chromatograms during ozonation kinetics: (a) lake Hohlohsee, (b) river Rhine, and (c) WWTP effluent.

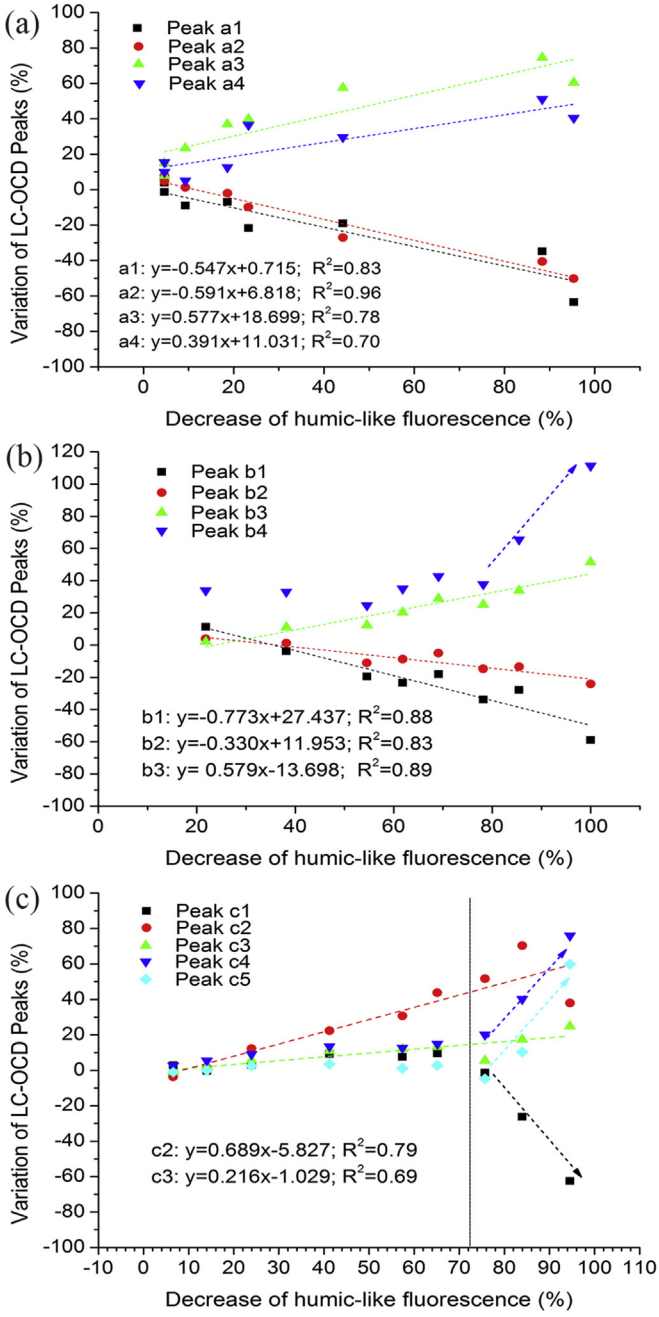

Fig. 6. The increase or decrease of LC-OCD chromatogram peaks as a function of the decrease of humic-like fluorescence during ozonation kinetics: (a) lake Hohlohsee, (b) river Rhine, and (c) WWTP effluent.

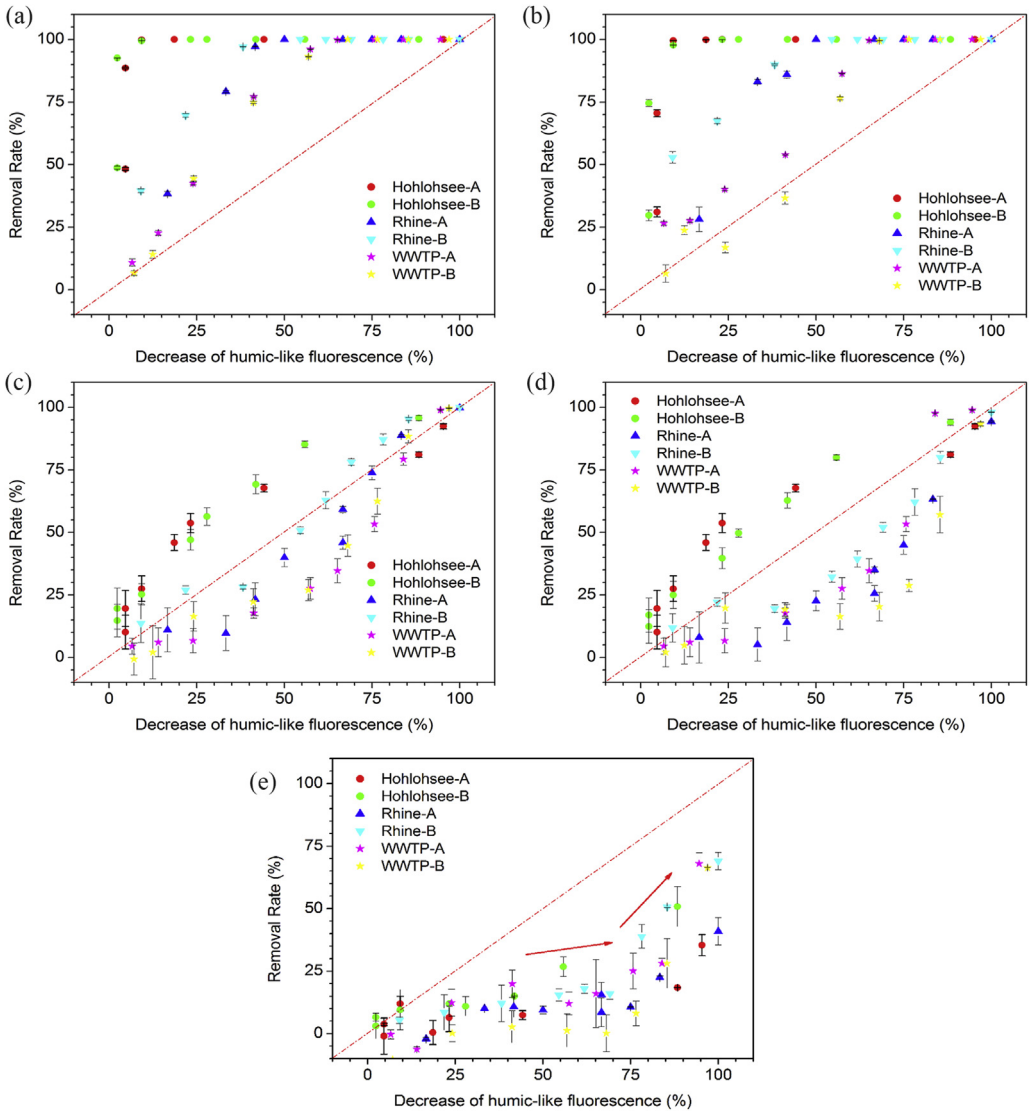

Fig. 7. Degradation of representative TOrCs in relation with removal of humic-like fluorescence: (a) group I, carbamazepine; (b) group II, gemfibrozil; (c) group III, DEET; (d) group IV, atrazine and (e) group V, TCPP.

the chromatogram peaks at 28–30 min and 34–43 min were decreasing, while the chromatogram peaks at 45–50 min and 52–54 min were increasing against ozone contact time. Similarly, for the Rhine series, the synchronous correlation analysis showed that the chromatogram peaks b1 (27–31 min, > 40 kDa) and b2 (39–44 min, 8–3 kDa) were decreasing while peaks b3 (47–50 min, 2.1–1.3 kDa) and b4 (53–55 min, 0.8–0.6 kDa) were increasing along ozonation time. For the WWTP series, it indicated that only peak c1 (27–32 min, > 20 kDa) decreased and the other peaks increased, including c2 (34–40 min, 17–6 kDa), c3 (42–46 min, 5–2.5 kDa), c4 (47–50 min, 2.1–1.3 kDa) and c5 (52.5–55.5 min, 0.9–0.5 kDa). The LC-OCD chromatograms combined with 2D synchronous correlation analysis clearly demonstrated how the large MW DOM components were transformed into small MW species during ozonation.

3.2.3. *Relationships between changes in MW and fluorescence signals*

Fig. 6 illustrates the increase or decrease of LC-OCD chromatogram peaks as a function of the decrease of humic-like fluorescence during ozonation. With reduction of humic-like fluorescence, there were apparent opposite variation trends between large and small DOM species. For lake Hohlohsee and river Rhine water matrices, it can be observed that the large MW DOM (low retention time) species were linearly decreasing with removal of humic-like fluorescence, while the small MW species (high retention time) were increasing in good correlation with decreasing of humic-like fluorescence. For the WWTP matrix, only two mediate MW species were observed linearly increasing. Due to their relatively high DOC concentration, the ozonation of wastewater effluents generally has two stages: the initial O_3 demand phase (IOD) or after first-order O_3 decay phase (Wert et al., 2009). During IOD phase, O_3 was rapidly consumed by the effluent organic matter with relatively few •OH radicals produced. Inferred from the LC-OCD profiles (Fig. S5-c), the large MW peak c1 was only slightly shifting in this stage. It indicates that although the initial reaction significantly attacked the aromatic structure of chromophores or fluorophores, the molecular structure of effluent organic matter was not sufficiently broken. During the following O_3 decay phase, the peak c1 and the other peaks were deviating (Fig. 6-c). This can be explained by the exposure of O_3 and the produced •OH radicals, which began to substantially break the large MW DOM into small MW species. The

newly formed small MW moieties typically consist of oxygen-containing organic compounds such as organic acids, aldehydes and ketones, which are easily biodegradable (Hammes et al., 2006). Due to the limited DOC removal and largely unidentified transformation products during ozonation, biofiltration systems such as biological activated carbon filtration and biological sand filtration have often been preferred for further water polishing (Hollender et al., 2009; Reungoat et al., 2012). Additional research is needed here to explore the relationships between the spectral indicators and the increased assimilable organic carbon for DOC removal during the following biological filtration process.

3.3. Elimination patterns of TOrCs

The TOrCs were grouped according to their reactivity with ozone and •OH, as described in Table 1. Fig. 7 shows the elimination percentage of the selected micropollutants from each group (carbamazepine for group I, gemfibrozil for group II, DEET for group III, atrazine for group IV, and TCPP for group V) as a function of the decrease of humic-like fluorescence. The elimination profiles of all 14 TOrCs are shown in SI Fig. S6.

For group I and II, the TOrCs degradation plots were relatively steep. When the reduction of humic-like fluorescence reached up to 50%, most of these TOrCs were sufficiently eliminated below the method detection limit regardless of water matrices, which are in accordance with previous literature (Gerrity et al., 2012). For the WWTP matrix, a high elimination efficiency was observed within the initial ozonation demand phase, supporting that the degradation of group I and II compounds could be mainly attributed to their high apparent reaction rate with ozone ($k\_O_3 > 10^3$ M^{-1} s^{-1}, Table 1) (Lee et al., 2013). Additionally, most of the points in Fig. 7-a and b are located above the auxiliary 1:1 diagonals, implying that these TOrCs reacted more quickly with ozone than chromophores or fluorophores in DOM.

For groups III and IV, the elimination of these TOrCs was relatively slower than that of group I and II, which is consistent with their lower k_O_3 values (<10 M^{-1} s^{-1}, Table 1). Hence reactions with •OH are expected to dominate to the degradation of these TOrCs (Gerrity et al., 2012; Lee et al., 2013). These TOrCs exhibited similar elimination patterns and scattered around the 1:1 diagonals with removal rates in the range of 25–75%, indicating that these TOrCs were reduced at similar rates as humic-like fluorescence, although there were slight lags at initial stages. This phenomenon can be elucidated by their similar k_•OH values (>10^9 M^{-1} s^{-1}, Table 1). Compared to ozone specifically reacting with electron rich matter, the •OH radical is a relatively nonselective oxidant, which reacts rapidly with almost any type of organic moieties even including aliphatic C–H bonds (Lee and von Gunten, 2012; Noethe et al., 2009). Hence complete reduction of humic-like fluorescence results in complete elimination of the TOrCs in Group III and IV.

For the elimination of the flame retardant TCPP representative for group V, a plateau was observed until the humic-fluorescence reached to a reduction of 75%, and then only consistently increased. The lag plateau could be explained by its low k_O_3 and moderate k_•OH values. Especially for WWTP matrix, ozone was initially consumed by DOM and little •OH radical was produced. Even though the humic-like fluorescence was almost completely reduced, the elimination of TCPP was only around 50%.

The linear regression parameters of TOrCs' removal as a function of spectral signals during WWTP batch kinetics experiments were further summarized as shown in Table 2. The regression slopes of UVA280 were generally over 2.1 for TOrCs in groups I and II, while they were in the range of 1.2–1.5 for TOrCs in groups III and IV. The regression slopes of fluorescence signals were mostly over 1.3 for TOrCs in groups I and II, while they were around 1 for TOrCs in group III and IV. These phenomena were consistent with the regression results using UVA254 and total fluorescence (Gerrity et al., 2012). This can be explained by their kinetic reaction models, which indicate that fluorophores were more susceptible to oxidation than the total chromophores. As results, the protein-like and humic-like fluorescence signals had similar regression parameters and their regression slopes were lower than those of UV absorbance.

Compared with lake Hohlohsee and river Rhine matrices, the higher DOM concentration of WWTP effluent resulted in the lags of TOrCs degradation. However, it is the reactivity of TOrCs that significantly determined their elimination patterns during ozonation. Recently, the quantitative structure-activity relationships (QSAR) analysis has been proposed to predict the reaction rate constants *k*-values for various emerging TOrCs (Jin et al., 2015; Lee and von Gunten, 2012). It is expected that the combination of QSAR & *k*-values & group classification methods & LED spectral sensors might be a promising solution for the online estimation of various TOrCs degradation during AOPs.

4. Conclusions

The newly miniaturized LED UV fluorescence sensor is

Table 2
Regression parameters between removal of TOrCs and reduction of LED UV fluorescence signals.

TOrCs		WWTP/*n*	UVA280			Protein-like fluorescence			Humic-like fluorescence		
Group	Contaminants		Slope	Intercept	R^2	Slope	Intercept	R^2	Slope	Intercept	R^2
I	Bisphenol-A	A&B/18	1.18	21.13	0.86	0.87	18.08	0.93	0.92	16.00	0.94
I	Carbamazepine	A&B/11	2.67	0.53	0.91	1.79	0.43	0.97	1.71	0.95	0.98
I	Diclofenac sodium	A&B/10	2.74	9.34	0.84	1.72	11.85	0.86	1.65	12.40	0.87
I	Sulfamethoxazole	A/6	2.21	6.60	0.97	1.51	9.26	0.95	1.47	8.87	0.96
		B/6	2.39	10.94	0.83	1.52	9.34	0.94	1.45	10.17	0.95
I	Triclosan	A&B/8	3.19	13.35	0.92	2.09	15.31	0.98	1.97	16.60	0.98
I	Trimethoprim	A&B/11	2.54	7.49	0.87	1.72	7.03	0.94	1.65	7.49	0.95
II	Atenolol	A&B/14	2.11	−7.45	0.88	1.37	−7.00	0.92	1.37	−7.81	0.92
II	Gemfibrozil	A&B/13	2.21	1.65	0.93	1.36	4.80	0.90	1.35	4.11	0.91
III	DEET	A&B/18	1.44	−11.53	0.95	1.00	−12.81	0.93	1.04	−13.98	0.89
III	Ibuprofen	A&B/14	1.34	−3.21	0.83	0.93	−4.56	0.74	0.98	−6.82	0.71
III	Phenytoin	A&B/18	1.53	−16.68	0.88	1.08	−18.54	0.88	1.10	−19.30	0.83
III	Primidone	A&B/18	1.30	−6.22	0.92	0.89	−6.43	0.86	0.92	−7.40	0.83
IV	Atrazine	A&B/18	1.26	−9.83	0.79	0.88	−10.99	0.78	0.90	−11.50	0.73
V	TCPP	A&B/18	0.84	−14.89	0.74	0.56	−14.07	0.65	0.58	−14.73	0.63

The removals of TOrCs were correlated as a function of the reduction of spectra signals, respectively.
n represents the number of data used for regression.

promising for online monitoring the degradation of chromophore and fluorophores with good sensitivity and accuracy.

The degradation of chromophores and fluorophores in WWTP effluent complied with the second order kinetic models during ozonation. The protein-like and humic-like fluorophores, which showed similar reaction rates, were more prone to oxidation than chromophores.

The LC-OCD chromatograms combined with 2D synchronous correlation analysis visualized how the large MW DOM components were transformed into small MW moieties during ozonation. The variation of DOM could be well correlated with the reduction of humic-like fluorescence.

The elimination patterns of TOrCs during ozonation were mainly determined by their reactivity with O_3 and hydroxyl radicals. At approximately 50% reduction of humic-like fluorescence almost complete oxidation of TOrCs of group I and II was reached, a similar removal percentage (25–75%) of TOrCs of group III and IV, and a poor removal percentage (<25%) of group V.

Acknowledgements

We thank the generous support from 2015 International Humic Substances Society (IHSS) Training Award for the training activity of Wentao Li (liwentaonju@163.com) at Karlsruhe Institute of Technology.

We also gratefully acknowledge Program for Changjiang Scholars and Innovative Research Team in University, National Science Foundation of China (51290282, 51378251) and Scientific Research Foundation of Graduate School of Nanjing University (2014CL08), which support the development of LED UV fluorescence sensors.

We gratefully thank Prof. Hai Lu, Dr. Chen-Fei Wu, Mr. Wang-Hao Tian, Mr. Tong-Kui Su, Mr. Qi-Duan Li from School of Electronic Science and Engineering and Mr. Jun-Yu Pei, Ms. Yin-Ping Ma from department of computer science and engineering at Nanjing University for their contributions to the development of LED UV fluorescence sensors. The first author Wentao Li also thanks the scholarship from Shanghai Tongji Gao Tingyao Environmental Science & Technology Development Foundation (STGEF).

Appendix A. Supplementary data

Supplementary data related to this article can be found at http://dx.doi.org/10.1016/j.watres.2016.05.090.

References

Anumol, T., Sgroi, M., Park, M., Roccaro, P., Snyder, S.A., 2015. Predicting trace organic compound breakthrough in granular activated carbon using fluorescence and UV absorbance as surrogates. Water Res. 76, 76–87.

Barsotti, F., Ghigo, G., Vione, D., 2016. Computational assessment of the fluorescence emission of phenol oligomers: a possible insight into the fluorescence properties of humic-like substances (HULIS). J. Photoch. Photobio. A-Chem. 315, 87–93.

Behera, S.K., Kim, H.W., Oh, J.-E., Park, H.-S., 2011. Occurrence and removal of antibiotics, hormones and several other pharmaceuticals in wastewater treatment plants of the largest industrial city of Korea. Sci. Total Environ. 409 (20), 4351–4360.

Bridgeman, J., Baker, A., Brown, D., Boxall, J.B., 2015. Portable LED fluorescence instrumentation for the rapid assessment of potable water quality. Sci. Total Environ. 524–525, 338–346.

Carstea, E.M., Baker, A., Bieroza, M., Reynolds, D., 2010. Continuous fluorescence excitation-emission matrix monitoring of river organic matter. Water Res. 44 (18), 5356–5366.

Carstea, E.M., Bridgeman, J., Baker, A., Reynolds, D.M., 2016. Fluorescence spectroscopy for wastewater monitoring: a review. Water Res. 95, 205–219.

Chin, Y.-P., Aiken, G., O'Loughlin, E., 1994. Molecular weight, polydispersity, and spectroscopic properties of aquatic humic substances. Environ. Sci. Technol. 28 (11), 1853–1858.

Chon, K., Salhi, E., von Gunten, U., 2015. Combination of UV absorbance and electron donating capacity to assess degradation of micropollutants and formation of bromate during ozonation of wastewater effluents. Water Res. 81, 388–397.

Dickens, J.E., Vaughn, M.S., Taylor, M., Ponstingl, M., 2011. An LED array-based light induced fluorescence sensor for real-time process and field monitoring. Sens. Actuat. B-Chem. 158 (1), 35–42.

Dickenson, E.R.V., Drewes, J.E., Sedlak, D.L., Wert, E.C., Snyder, S.A., 2009. Applying surrogates and indicators to assess removal efficiency of trace organic chemicals during chemical oxidation of wastewaters. Environ. Sci. Technol. 43 (16), 6242–6247.

Frimmel, F.H., Abbt-Braun, G., Heumann, K.G., Hock, B., Lüdemann, H.-D., Spiteller, M., 2002. Refractory Organic Substances (ROS) in the Environment, pp. 302–309. John Wiley and Sons, New York.

Gerrity, D., Gamage, S., Jones, D., Korshin, G.V., Lee, Y., Pisarenko, A., Trenholm, R.A., von Gunten, U., Wert, E.C., Snyder, S.A., 2012. Development of surrogate correlation models to predict trace organic contaminant oxidation and microbial inactivation during ozonation. Water Res. 46 (19), 6257–6272.

Hammes, F., Salhi, E., Koester, O., Kaiser, H.-P., Egli, T., von Gunten, U., 2006. Mechanistic and kinetic evaluation of organic disinfection by-product and assimilable organic carbon (AOC) formation during the ozonation of drinking water. Water Res. 40 (12), 2275–2286.

He, X.-S., Xi, B.-D., Zhang, Z.-Y., Gao, R.-T., Tan, W.-B., Cui, D.-Y., 2014. Insight into the evolution, redox, and metal binding properties of dissolved organic matter from municipal solid wastes using two-dimensional correlation spectroscopy. Chemosphere 117, 701–707.

Henderson, R.K., Baker, A., Murphy, K.R., Hamblya, A., Stuetz, R.M., Khan, S.J., 2009. Fluorescence as a potential monitoring tool for recycled water systems: a review. Water Res. 43 (4), 863–881.

Hollender, J., Zimmermann, S.G., Koepke, S., Krauss, M., McArdell, C.S., Ort, C., Singer, H., von Gunten, U., Siegrist, H., 2009. Elimination of organic micropollutants in a municipal wastewater treatment plant upgraded with a full-scale post-ozonation followed by sand filtration. Environ. Sci. Technol. 43 (20), 7862–7869.

Huber, M.M., Canonica, S., Park, G.Y., Von Gunten, U., 2003. Oxidation of pharmaceuticals during ozonation and advanced oxidation processes. Environ. Sci. Technol. 37 (5), 1016–1024.

Huber, S.A., Frimmel, F.H., 1991. Flow-injection analysis of organic and inorganic carbon in the low-ppb range. Anal. Chem. 63 (19), 2122–2130.

Jelic, A., Gros, M., Ginebreda, A., Cespedes-Sánchez, R., Ventura, F., Petrovic, M., Barcelo, D., 2011. Occurrence, partition and removal of pharmaceuticals in sewage water and sludge during wastewater treatment. Water Res. 45 (3), 1165–1176.

Jin, X., Peldszus, S., Huck, P.M., 2015. Predicting the reaction rate constants of micropollutants with hydroxyl radicals in water using QSPR modeling. Chemosphere 138, 1–9.

Lee, Y., Gerrity, D., Lee, M., Bogeat, A.E., Salhi, E., Gamage, S., Trenholm, R.A., Wert, E.C., Snyder, S.A., von Gunten, U., 2013. Prediction of micropollutant elimination during ozonation of municipal wastewater effluents: use of kinetic and water specific information. Environ. Sci. Technol. 47 (11), 5872–5881.

Lee, Y., von Gunten, U., 2012. Quantitative structure-activity relationships (QSARs) for the transformation of organic micropollutants during oxidative water treatment. Water Res. 46 (19), 6177–6195.

Li, W.-T., Chen, S.-Y., Xu, Z.-X., Li, Y., Shuang, C.-D., Li, A.-M., 2014. Characterization of dissolved organic matter in municipal wastewater using fluorescence PARAFAC analysis and chromatography multi-excitation/emission scan: a comparative study. Environ. Sci. Technol. 48 (5), 2603–2609.

Li, W.-T., Jin, J., Li, Q., Wu, C.-F., Lu, H., Zhou, Q., Li, A.-M., 2016. Developing LED UV fluorescence sensors for online monitoring DOM and predicting DBPs formation potential during water treatment. Water Res. 93, 1–9.

Li, W.-T., Xu, Z.-X., Li, A.-M., Wu, W., Zhou, Q., Wang, J.-N., 2013a. HPLC/HPSEC-FLD with multi-excitation/emission scan for EEM interpretation and dissolved organic matter analysis. Water Res. 47 (3), 1246–1256.

Li, W., Nanaboina, V., Zhou, Q., Korshin, G.V., 2013b. Changes of excitation/emission matrixes of wastewater caused by Fenton- and Fenton-like treatment and their associations with the generation of hydroxyl radicals, oxidation of effluent organic matter and degradation of trace-level organic pollutants. J. Hazard. Mater 244, 698–708.

Li, W., Xu, Z., Wu, Q., Li, Y., Shuang, C., Li, A., 2015. Characterization of fluorescent-dissolved organic matter and identification of specific fluorophores in textile effluents. Environ. Sci. Pollut. Res. 22 (6), 4183–4189.

Nanaboina, V., Korshin, G.V., 2010. Evolution of absorbance spectra of ozonated wastewater and its relationship with the degradation of trace-level organic species. Environ. Sci. Technol. 44 (16), 6130–6137.

Noda, I., Ozaki, Y., 2005. Two-dimensional Correlation Spectroscopy: Applications in Vibrational and Optical Spectroscopy. John Wiley & Sons.

Noethe, T., Fahlenkamp, H., von Sonntag, C., 2009. Ozonation of wastewater: rate of ozone consumption and hydroxyl radical yield. Environ. Sci. Technol. 43 (15), 5990–5995.

Reungoat, J., Escher, B.I., Macova, M., Argaud, F.X., Gernjak, W., Keller, J., 2012. Ozonation and biological activated carbon filtration of wastewater treatment plant effluents. Water Res. 46 (3), 863–872.

Reungoat, J., Macova, M., Escher, B.I., Carswell, S., Mueller, J.F., Keller, J., 2010. Removal of micropollutants and reduction of biological activity in a full scale reclamation plant using ozonation and activated carbon filtration. Water Res. 44 (2), 625–637.

Schwarzenbach, R.P., Escher, B.I., Fenner, K., Hofstetter, T.B., Johnson, C.A., Von

Gunten, U., Wehrli, B., 2006. The challenge of micropollutants in aquatic systems. Science 313 (5790), 1072–1077.
Sui, Q., Huang, J., Deng, S., Yu, G., Fan, Q., 2010. Occurrence and removal of pharmaceuticals, caffeine and DEET in wastewater treatment plants of Beijing, China. Water Res. 44 (2), 417–426.
Tedetti, M., Joffre, P., Goutx, M., 2013. Development of a field-portable fluorometer based on deep ultraviolet LEDs for the detection of phenanthrene- and tryptophan-like compounds in natural waters. Sens. Actuat. B-Chem. 182, 416–423.
von Gunten, U., 2003. Ozonation of drinking water: Part I. Oxidation kinetics and product formation. Water Res. 37 (7), 1443–1467.
Watts, M.J., Linden, K.G., 2009. Advanced oxidation kinetics of aqueous trialkyl phosphate flame retardants and plasticizers. Environ. Sci. Technol. 43 (8), 2937–2942.
Wenk, J., Aeschbacher, M., Salhi, E., Canonica, S., von Gunten, U., Sander, M., 2013. Chemical oxidation of dissolved organic matter by chlorine dioxide, chlorine, and ozone: effects on its optical and antioxidant properties. Environ. Sci. Technol. 47 (19), 11147–11156.
Wert, E.C., Neemann, J.J., Rexing, D.J., Zegers, R.E., 2008. Biofiltration for removal of BOM and residual ammonia following control of bromate formation. Water Res. 42 (1–2), 372–378.
Wert, E.C., Rosario-Ortiz, F.L., Snyder, S.A., 2009. Using ultraviolet absorbance and color to assess pharmaceutical oxidation during ozonation of wastewater. Environ. Sci. Technol. 43 (13), 4858–4863.